*Characterization and Application of Nanomaterials (2020) Volume 3 Issue 1*
doi:10.24294/can.v3i1.580

ORIGINAL RESEARCH ARTICLE

# Effects of different preparing conditions and annealing on the photocatalytic activity of hydrothermal grown $BiVO_4$

**Yuxiang Wen, Wei Ji, Jiang Yu, Qichang An, Tianfen Qin, Zhiya Zhang, Jiachi Zhang*, Shanglong Peng***

**Key Laboratory for Magnetism and Magnetic Materials of the Ministry of Education, School of Physical Science and Technology, Lanzhou University, Lanzhou 730000, Gansu province, China.*
**E-mail: pengshl@lzu.edu.cn. E-mail: zhangjch@lzu.edu.cn*

## ABSTRACT

$BiVO_4$ was hydrothermally synthesized under different preparing conditions and characterized by XRD, SEM, Raman spectrum and BET specific surface area. The influence of different pH value and annealing temperature and hydrothermal time on the morphologies and structures of the $BiVO_4$ samples was investigated systematically. It can be found that annealing would eliminate the effects caused by the pH of precursor, heating temperature and heating time, but preparing conditions still influenced the size and specific surface area of samples. Furthermore, the photocatalytic activities of the fabricated $BiVO_4$ were also evaluated by the degradation of methyl blue in aqueous solution under UV and visible light irradiation.

***Keywords:*** Bismuth Vanadate; Photocatalytic Activity; Morphology; Hydrothermal; Preparing Conditions

**ARTICLE INFO**

Article history:
Received 15 February 2020
Received in revised form 12 March 2020
Accepted 15 March 2020
Available online 27 March 2020



## 1. Introduction

With the huge consumption of traditional fossil fuels in the past several centuries, such as coal, crude oil and natural gas, human beings are now confronting a great energy crisis and environmental pollution issues. Accordingly, the development of semiconductor photocatalysts for organic pollutant degradation and water splitting has been regarded as an efficient, green and promising solution to energy replacement and environmental decontamination[1-5]. Among various semiconductor materials, $TiO_2$ has been regarded as one of the most promising photocatalysts owing to its large exciton binding energy, high chemical stability, non-toxicity and abundant availability[6,7]. However, its large band gap (~3.0 eV for rutile and 3.2 eV for anatase) means that $TiO_2$ is only active in the ultraviolet (UV) region, which accounts for less than 5% of the total energy of the solar spectrum[8,9]. In the past few decades, many researchers have focused their efforts on redeveloping visible-light-driven $TiO_2$-based photo-catalysts with high efficiency[10,11]. For example, Asahi *et al.*[12] and Khan *et al.*[13] reported that doping $TiO_2$ with nitrogen or carbon can narrow its band gap, and Putnam *et al.*[14] and Brezova *et al.*[15] reported that doping $TiO_2$ with metal ions extends light absorption into visible region. Nevertheless, as for the doped $TiO_2$ photocatalysts, the dopants may likely act as recombination centers for the photogenerated electrons and holes, resulting in lower quantum efficiency compared to undoped semicon ductor photocatalysts[16,17].

Bismuth vanadate ($BiVO_4$) has long been recognized as an important semiconductor photocatalyst, owning excellent photocatalytic performance under visible light illumination due to its narrow band gap (2.4 eV)[18-22]. There are three reported crystalline phases for synthetic $BiVO_4$, zircon structure with tetragonal system (z-t) and scheelite structure with monoclinic (s-m) and tetragonal (s-t) systems[23]. Therefore, many researchers focus their efforts on the photo-physical and photo-catalytic properties of $BiVO_4$ strongly influenced by its crystal form and preparation methods such as solid-state reaction[24,25], aqueous process[12,26-28], hydrothermal approach[29-32], chemical bath deposition[33,34], metal-organic decomposition[35], and sono-chemical method[35]. The architectural control of nano- and micro-crystals is an attractive and challenging goal of modern materials chemistry[36]. To this end, several exceptional structures, such as 1D $BiVO_4$ nanofibers, rod-like $BiVO_4$ and 2D $BiVO_4$ nanosheets, have been successfully fabricated by hydrothermal methods[37-39]. With these advanced processes, different surfactants or additives and complex treatments were necessary in order to obtain the desired morphologies and crystal structures[4,23,40,41]. Considering the properties and applications are closely related to the microstructure and corresponding synthetic techniques and processes, it is of great importance to study the controllable synthesis of $BiVO_4$ with the desired crystalline phase and morphology.

In this work, $BiVO_4$ has been synthetized by a hydrothermal approach. The photocatalytic activities of $BiVO_4$ prepared via different conditions were compared via the decomposition of methylene blue (MB) under UV and visible light irradiation. Also, the relationship between photocatalytic performance and fabrication parameters of $BiVO_4$ has been systematically investigated.

## 2. Experimental procedure

All the reagents used in the experiment are analytical grade without further purification.

### 2.1 Fabrication of $BiVO_4$

In a typical synthesis, 5.0 mmol Ammonium metava-nadate ($NH_4VO_3$) and 5.0 mmol Bismuth nitrate pentahy-drate ($Bi(NO_3)_3 \cdot 5H_2O$) were dissolved in 60.0 ml 1.0 M $HNO_3$ solution, stirring to obtain orange precipitate. The diluted ammonia water was then added for adjusting the pH value to 6. After stirring for 0.5 h, the solution was moved to 100 ml of Teflon-lined stainless steel autoclave and heated to 80°C, 100°C, 120°C, 140°C, 160°C, 180°C, and 200°C for 8 h under autogenous pressure, respectively. When cooled down to room temperature naturally, the yellow precipitate was obtained by centrifugation, wished with distilled water and absolute alcohol, and dried at 80°C in an electric oven for 8 h. The dried samples were heated from room temperature to 600°C at a constant rate within 2 h in the sintering furnace and annealed at 600°C for 2 h. After the temperature dropped to 300°C within 1 h, the samples were cooled down to room temperature naturally. The optimal preparation conditions were investigated by the influence of adjusting the hydrothermal temperature, the pH value of precursor (2, 4, 6, 8, 10, 12) and the hydro-thermal time (4 h, 6 h, 8 h, 12 h) on the photocatalytic activities.

### 2.2 Measurement of photocatalytic activities

Photocatalytic activities of the $BiVO_4$ powders were evaluated by the degradation of methyl blue (MB) under visible light irradiation ($\lambda > 420$ nm) using a 500 W Xe lamp with a 420 nm cut-off filter. In a typical run, 50 mg of samples was added to 50 ml of MB solution ($1\times10^{-5}$ mol/L). Prior to irradiation, the suspensions were stirred in the dark for 1 h to reach an adsorption/desorption equilibrium between the MB and photocatalyst. Under irradiation, the suspensions were stirred continually and open to air. At regular intervals, 4 ml of the suspensions were collected, and then centrifuged to remove the photocatalyst particles. These solutions were used to evaluate photocatalytic activities of the $BiVO_4$ powders by monitoring the absorbance at 554 nm with a UV-vis spectrophotometer (Shimadzu UV-3600).

### 2.3 Material characterization

The microstructure and morphology were investigated by using field emission scanning electron microscope (FE-SEM, Hitachi S-4800) and transmission electron microscopy (TEM, FEI Tecnai G2 F30 microscope operated at 300 KV). XRD measurements were performed on a Rigaku D/MAX-2400 X-ray diffractometer using Cu Kα radiation (λ = 0.154056 nm). The chemical component was analyzed on a micro-Raman spectroscope (JY-HR800, 532-nm wavelength YAG laser).

## 3. Results and discussion

### 3.1 Powders formation

The $BiVO_4$ samples were produced by the hydrothermal method and followed by annealing at 600°C. **Figure 1** shows the XRD patterns of $BiVO_4$ powders synthesized under different conditions. The difference in the XRD patterns between tetragonal and monoclinic $BiVO_4$ can be mainly judged by the existence of peaks (200) and (121) and the existence of a peak at 15°C and the split of peaks at 18.5°C and 35°C. The percentage of monoclinic phase can be given by the following equation:

$$\eta_{mono} = \frac{I_{mono(121)}}{I_{mono(121)} + I_{tetra(200)}}$$

Where $\eta_{mono}$ denotes the percentage of the monoclinic phase, $I_{mono(121)}$ is the relative intensity of the (121) peak, and $I_{tetra(200)}$ is the relative intensity of the (200) peak.

As shown in **Figure1(a)**, $BiVO_4$ is monoclinic (PDF 75-1866) for the samples (c, d and e)[42]. As the pH decreases to 6 and 4, the tetragonal $BiVO_4$ appears (PDF 14–0133)[43]. These results indicate that the dissolution and the recrystallization happening in the low pH solution contribute to the phase transformation of the monoclinic type into the tetragonal type. The monoclinic $BiVO_4$ is thermodynamically more stable than that of tetragonal $BiVO_4$ at room temperature, and a sudden decrease in pH can affect the structure and morphology of powders resulting the formation of the tetragonal $BiVO_4$[44].

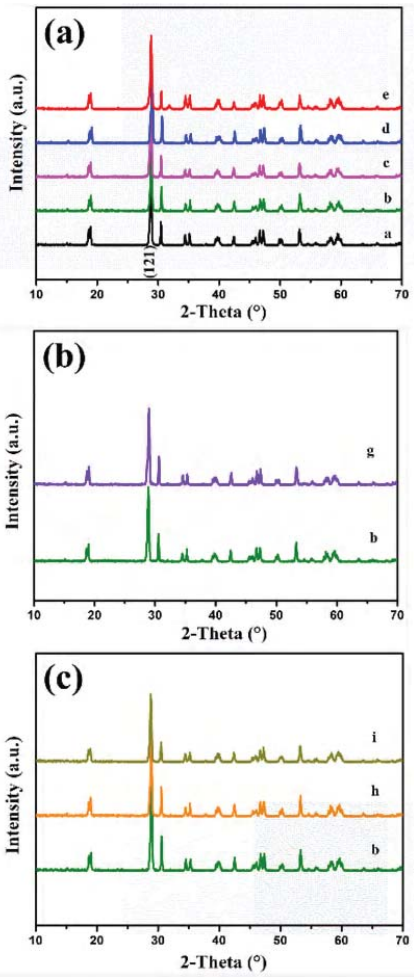


**Figure 1.** The XRD pattern of powders obtained from different conditions: **(a)** different pH values. **(b)** different heating temperature. **(c)** different heating time**.**

Similarly, as shown in **Figure 1(b)**, the samples (g and b) synthesized at 200°C and 180°C are monoclinic $BiVO_4$. As the temperature decreases to 160°C, the tetragonal $BiVO_4$ appears. Therefore, the $BiVO_4$ phase transition can be changed from monoclinic to tetragonal by adjusting preparation conditions. And the stable $BiVO_4$ is mainly related to the following chemical reactions[3]:

$Bi(NO_3)_3 + H_2O \Leftrightarrow 2HNO_3 + BiONO_3$

$BiONO_3 + VO_3^- \Leftrightarrow BiVO_4 + NO_3^-$

At the beginning, the reactants are soluble in concentrated nitric acid without precipitate. $Bi(NO_3)_3$ reacted gradually with water to form slightly soluble $BiONO_3$. And then, the newly formed $BiONO_3$ re-

acted with $VO_3^-$, forming yellow $BiVO_4$ powders. Furtherly, the samples without the high temperature annealing are a mixture of tetragonal and monoclinic $BiVO_4$. In **Figure 1(c)**, the samples (b, h and i) with different structure transit into monoclinic structure after high temperature annealing, indicating that $BiVO_4$ change from the tetragonal phase to the monoclinic phase by using high temperature annealing. **Table 1** shows the preparation conditions and percentage of monoclinic $BiVO_4$ powders ($\eta_{mono}$) of different samples, and the value of $\eta_{mono}$ for each sample is 100%, which is accordance with the result in **Figure 1(c)**. The detailed parameters of these samples from different conditions are shown in **Table 1**.

**Table 1.** The preparation conditions and percentage of monoclinic $BiVO_4$ powders ($\eta_{mono}$) of different samples

| **Preparation conditions** | a | b | c | d | e | f | g | h | i |
|---|---|---|---|---|---|---|---|---|---|
| **pH values of precursor** | 4 | 6 | 8 | 10 | 12 | 6 | 6 | 6 | 6 |
| **Heating temperature (°C)** | 180 | 180 | 180 | 180 | 180 | 160 | 200 | 180 | 180 |
| **Heating time (h)** | 8 | 8 | 8 | 8 | 8 | 8 | 8 | 4 | 10 |
| **$\eta_{mono}$ (%)** | 100 | 100 | 100 | 100 | 100 | 100 | 100 | 100 | 100 |

## 3.2 Morphologies and structure of the $BiVO_4$ samples

The chemical composition and molecular structure of the $BiVO_4$ samples were analyzed by Raman spectra as shown in **Figure 2** and **Table 2**. An intense peak near 828 $cm^{-1}$ is assigned to the symmetric V-O stretching mode, and a weak shoulder near 707 $cm^{-1}$ is assigned to the anti-symmetric V-O stretching mode. The short peaks located at 367 $cm^{-1}$ and 324 $cm^{-1}$ are assigned to the symmetric and the anti-symmetric banding modes of vanadate anion, respectively. The peaks near 210 $cm^{-1}$ are assigned to the external modes (rotation/translation). With the increase of the precursor pH, these Raman peaks shift towards the lower wavenumber, which reveals that the short-range symmetry of the tetrahedral $VO_4$ becomes more regular[37]. Raman spectra are sensitive to the short-range order, the degree of crystallinity and so on. Therefore, Raman spectra embody the variation of preparation conditions. However, the Raman spectra of $BiVO_4$ samples prepared under different pH values change a little (**Figure 2**), which indicates the effects on the morphologies and structures of the samples can be eliminated by annealing at high temperature. These results are in accordance with the conclusion as shown in the XRD patterns. The strongest peak is located at the larger wavenumber and the value of the full width at half maximum is lower, indicating that the symmetry of tetrahedral $VO_4$ and the degree of crystallinity would be better after annealing treatment.

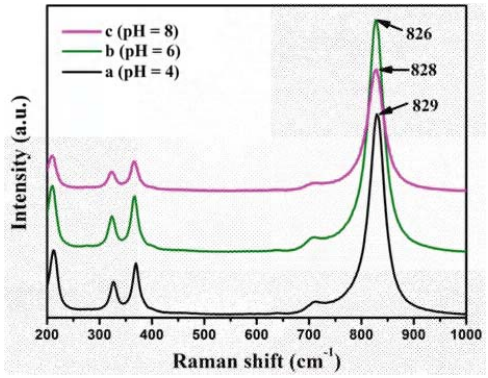


**Figure 2.** Raman spectra of the $BiVO_4$ samples prepared under different conditions.

**Table 2.** Assignment of Raman wavenumbers and specific surface areas observed from the samples obtained by hydrothermal method

| **Assignment** | **Sample a ($cm^{-1}$)** | **Sample b ($cm^{-1}$)** | **Sample c ($cm^{-1}$)** |
|---|---|---|---|
| $\nu_s$ (V—O) (FWHM) | 829 (36) | 827 (35) | 829 (38) |
| $\nu_{as}$ (V—O) | 711 | 709 | 712 |
| $\delta_s$ ($VO_4^{3-}$) | 369 | 367 | 366 |
| $\delta_{as}$ ($VO_4^{3-}$) | 326 | 324 | 322 |
| External mode | 212 | 210 | 210 |
| $A_{BET}$ ($m^2\,g^{-1}$) | 2.57 | 2.65 | 2.59 |

**Figure 3** shows the micrographs of the $BiVO_4$ samples prepared under different conditions. The samples present the similar morphologies of the peanuts-like particles after high temperature annealing corresponding to the analysis above. Nevertheless, it can be observed the difference between particles size and intensive degree. The results indicate the effects of reaction conditions on the structure and morphologies of the $BiVO_4$ samples can be eliminated by annealing, but these conditions still influence the particles size. The different specific surface areas of the

different samples are summarized in **Table 2**. The result also can reflect in SEM micrographs.

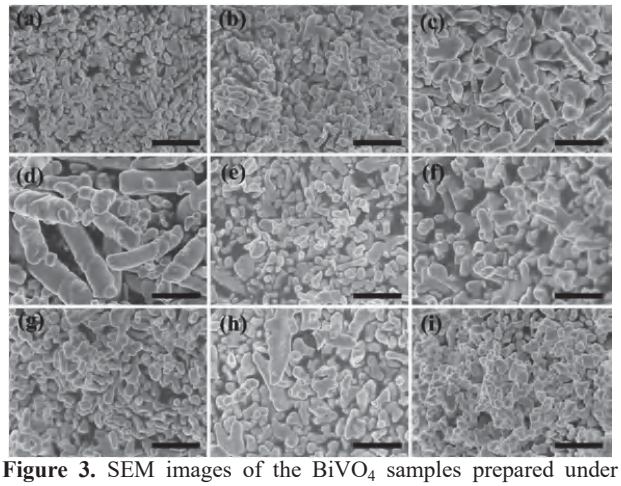


**Figure 3.** SEM images of the $BiVO_4$ samples prepared under different conditions, **(a)-(i)** corresponds to samples a-i in **Table 1**, respectively. The scale bar is the same for all 2 μm**.**

## 3.3 Photocatalytic activities

The photocatalytic activities of $BiVO_4$ samples were measured by the degradation of MB with a major absorption band at about 664 nm in a liquid medium under light irradiation.

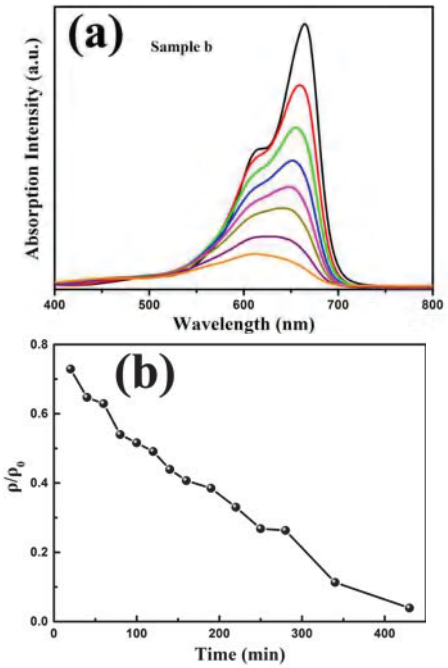


**Figure 4. (a)** UV-vis absorption spectrum of a stirred MB aqueous solution with the addition of sample b. **(b)** The photocatalytic degradation of MB in the presence of sample b with only visible light irradiation**.**

The temporal evolution of the spectral changes of MB mediated by the sample b, as shown in **Figure 4(a)**, exhibits that the absorption peak at 664 nm decreases gradually with irradiation time. Also the absorbance values of MB in the whole spectrum range from 400 to 800 nm are gradually reduced with increasing irradiation time, revealing the effectiveness and completeness of the photo-degradation of pollutants. **Figure 4(b)** presents the effect of degradation curve for the sample b under visible light irradiation (λ>420 nm), using a 500 W Xe lamp with a 420 nm cut-off filter. It can be observed that the monoclinic $BiVO_4$ has the ability of direct photolysis of MB as the increase of irradiation time.

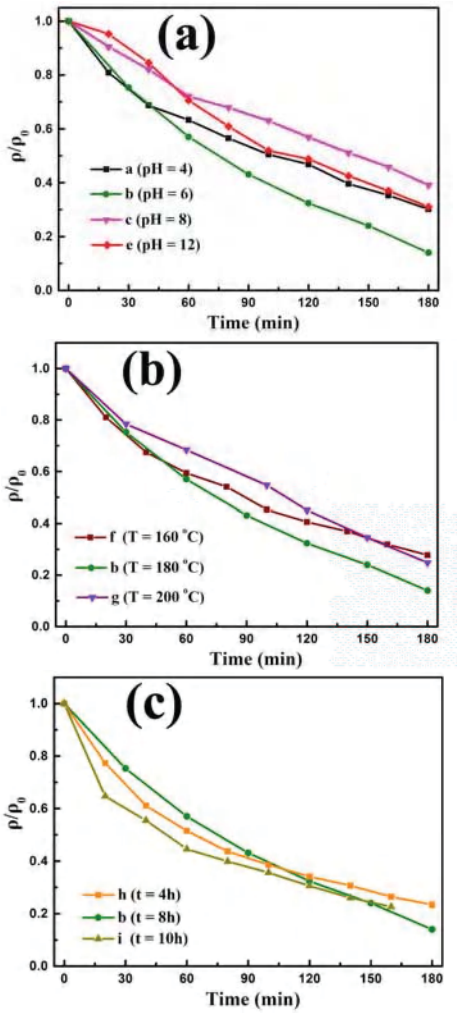


**Figure 5.** The photocatalytic degradation of MB with only visible light irradiation in the presence of different samples prepared under different conditions: **(a)** different pH values; **(b)** different heating temperature; **(c)** different heating time**.**

**Figure 5** shows the photocatalytic activities of different samples fabricated under different conditions. These curves reveal that the concentration of MB is a function of the irradiation time for different samples. Where $\rho_0$ is the initial concentration of MB solution, $\rho$ is the concentration of MB solution under light irradiation with t min. After light irradiation with 180 min, the concentration retention of MB degraded by different samples (a, b, c, e, f, g, h and i) are 29%, 14%, 39%, 31%, 28%, 25%, 23% and 22%, respectively. Obviously, the sample b (pH=6, heating temperature is 180°C for 8 h) is with the best photocatalytic activity, which is attributed to its wider bandgap.

In the heterogeneous catalytic reaction with plenty reactant, if the density of activity center on the catalyst surface is constant, the catalyst with the bigger specific surface will have the greater activities[19]. The specific surface area of photocatalyst is an important factor to decide photocatalytic reaction caused via photoinduced electron-hole pairs on the surface of photo-catalyst[18]. Therefore, the peanuts-like $BiVO_4$ nanoparticles have better photocatalyst activities than ordinary particles due to obvious quantum size effect, large specific surface area and high diffusion rate of photo-generated carriers[4,19]. Moreover, the wider photo-absorption range and better crystallinity caused by calcination effect are also favorable for its enhanced photocatalytic activity, resulting in the excellent photocatalytic performance of $BiVO_4$.

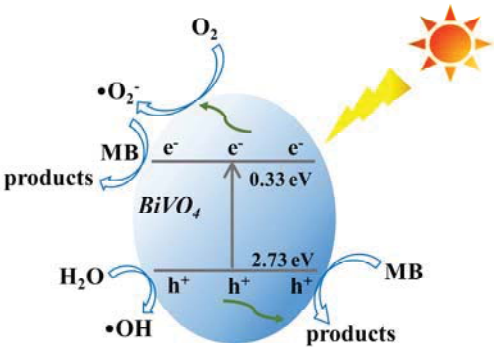


**Figure 6.** The schematic diagram of charge separation and photocatalytic process of the $BiVO_4$ photocatalysts under visible light irradiation.

Based on the reactive species trapping experiment results, a proposed mechanism for MB photocatalytic degradation by $BiVO_4$ photocatalysts is shown in **Figure 6**. The band gap of $BiVO_4$ is 2.4 eV[45]. Under visible light irradiation, the photo-generated electrons are occurred in the conduction band of the $BiVO_4$, photoinduced holes ($h^+$) are generated by the photoinduced transfer of electrons ($e^-$) in the $BiVO_4$, leading to an effective separation of the photo-generated electron-hole pairs. Along with the separated electrons and holes, the $e^-$ are scavenged by oxygen to form $\bullet O_2^-$ radicals, which can degrade MB effectively. Meanwhile, most of the $h^+$ can oxidize MB to its degradation products directly, and little further contact with $H_2O$ to produce hydro- xyl (•OH) radicals.

## 4. Conclusion

$BiVO_4$ has been synthesized successfully under different reaction conditions. And the fabricated $BiVO_4$ is the mixture of tetragonal and monoclinic $BiVO_4$ with different mix proportion. By adjusting the preparation conditions, the $BiVO_4$ phase changed from monoclinic phase to tetragonal phased. After high temperature annealing, the tetragonal phase all convert into the monoclinic phase. However, the different reaction conditions still affect the particles size and specific surface area of $BiVO_4$ samples. Moreover, it can be found that the photo-catalytic activities can be decided by the particles size and specific surface area of the samples.

## Acknowledgments

This work was financially supported by National Natural Science Foundation of China (Grant No. 61376011), the National Science Foundation for Fostering Talents in Basic Research of the National Natural Science Foundation of China (Nos. 041105 and 041106), and the Fundamental Research Funds for the Central Universities (No. lzujbky-2017-k21).

## References

1. Wang Y, Wang W, Mao H, *et al.* Electrostatic self-assembly of $BiVO_4$-reduced graphene oxide nano-

composites for highly efficient visible light photocatalytic activities. ACS Applied Materials & Inter faces 2014; 6(15): 12698–706.
2. Gu S, Li W, Wang F, *et al.* Synthesis of buckhorn-like $BiVO_4$ with a shell of CeOx nanodots: Effect of heterojunction structure on the enhancement of photocatalytic activity. Applied Catalysis B Environmental 2015; 170-171: 186–194.
3. Thalluri SM, Hernandez S, Bensaid S, *et al.* Green-synthesized W- and Mo-doped $BiVO_4$ oriented along the {0 4 0 facet with enhanced activity for the sun-driven water oxidation. Applied Catalysis B: Environmental 2016; 180: 630–636.
4. Gao X, Xu H, Yu J, *et al*. Controlled synthesis of $BiVO_4$ submicrospheres and their photocatalytic properties. Chemistry Letters 2015: 44(8): 1098–1100.
5. Li J, Cui M, Guo Z, *et al.* Synthesis of dumbbell-like CuO–$BiVO_4$ heterogeneous nanostructures with enhanced visible-light photocatalytic activity. Materials Letters 2014; 130: 36–39.
6. Ohno T, Akiyoshi M, Umebayashi T, *et al.* Preparation of S-doped $TiO_2$ photocatalysts and their photocatalytic activities under visible light. Applied Catalysis A: General 2004; 265(1): 115–121.
7. Zhang Y, Ma Q, Gao L, *et al.* Preparation and photoelectrochemical properties of nitrogen doped nanotubular $TiO_2$ arrays. Applied Surface Science 2013; 282: 174–180.
8. Shih YJ, Su CC, Chen CW, *et al.* Synthesis of magnetically recoverable ferrite ($MFe_2O_4$, M double bond Co, Ni and Fe)-supported $TiO_2$ photocatalysts for decolorization of methylene blue. Catalysis Communications 2015; 72: 127–132.
9. Ye J, Liu W, Cai J, *et al.* Nanoporous anatase $TiO_2$ mesocrystals: Additive-free synthesis, remarkable crystalline-phase stability, and improved lithium insertion behavior. Journal of the American Chemical Society 2011; 133(4): 933–940.
10. An H, Zhu B, Li J, *et al.* Synthesis and characterization of thermally stable nanotubular $TiO_2$ and itsphotocatalytic activity. The Journal of Physical Chemistry C 2008; 112(48): 18772–18775.
11. Tang Y, Wee P, Lai Y, *et al.* Hierarchical $TiO_2$ nanoflakes and nanoparticles hybrid structure for improved photocatalytic activity. The Journal of Physical Chemistry C 2012; 116(4): 2772–2780.
12. Asahi RT, Morikawa T, Ohwaki T, *et al*. Visible-light photocatalysis in nitrogen-doped titanium oxides. Science 2001; 293(5528): 269–271.
13. Khan SUM, Al-Shahry M, Ingler WB. Efficient photochemical water splitting by a chemically modified n-$TiO_2$. Science 2002; 297(5590): 2243–2245.
14. Putnam RL, Nakagawa N, Mcgrath KM, *et al*. Titanium dioxide−surfactant mesophases and Ti-TMS1. Chemistry of Materials 1997; 9(12): 2690–2693.
15. Brezova V, Blazkova A, Karpinsky L, *et al.* Phenol decomposition using $M^{n+}/TiO_2$ photocatalysts supported by the sol–gel technique on glass fibers. Journal of Photochemistry and Photobiology A: Chemistry 1997; 109(2): 177–183.
16. Bakar SA, Ribeiro C. Rapid and morphology controlled synthesis of anionic S-doped $TiO_2$ photocatalysts for the visible-light-driven photodegradation of organic pollutants. RSC Advances 2016; 6(43): 36516–36527.
17. Sakthivel S, Kisch H. Daylight photocatalysis by carbon-modified titanium dioxide. Angewandte Chemie International Edition 2003; 42(40): 4908–11.
18. Dong S, Feng J, Li Y, *et al.* Shape-controlled synthesis of $BiVO_4$ hierarchical structures with unique natural-sunlight-driven photocatalytic activity. Applied Catalysis B Environmental 2014; 152-153: 413–424.
19. Luo Y, Tan G, Dong G, *et al.* Effects of structure, morphology, and up-conversion on Nd-doped $BiVO_4$ system with high photocatalytic activity. Ceramics International 2015; 41(2): 3259–3268.
20. Ju P, Wang P, Li B, *et al.* A novel calcined $Bi_2WO_6$/$BiVO_4$ heterojunction photocatalyst with highly enhanced photocatalytic activity. Chemical Engineering Journal 2014; 236: 430–437.
21. Shi W, Yan Y, Yan X, *et al.* Microwave-assisted synthesis of nano-scale $BiVO_4$ photocatalysts and their excellent visible-light-driven photocatalytic activity for the degradation of ciprofloxacin. Chemical Engineering Journal 2013; 215-216: 740–746.
22. Guo M, He Q, Wang A, *et al.* A novel, simple and green way to fabricate $BiVO_4$ with excellent photocatalytic activity and its methylene blue decomposition mechanism. Crystals 2016; 6(7): 81.
23. Zhang X, Ai Z, Jia F, *et al.* Selective synthesis and visible-light photocatalytic activities of $BiVO_4$ with different crystalline phases. Materials Chemistry and Physics 2007; 103(1): 162–167.
24. Kudo A, Omori K, Kato H. A novel aqueous process for preparation of crystal form-controlled and highly crystalline $BiVO_4$ powder from layered vanadates at room temperature and its photocatalytic and photophysical properties. Journal of the American Chemical Society 1999; 121(49): 11459–67.
25. Chen H, Hu J, Xu B. Facile solid state method route synthesis and enhance visible light activities of $BiVO_4$ by doping Co. Key Engineering Materials 2016; 703: 316–320.
26. Tokunaga S, Kato H, Kudo A. Selective preparation of monoclinic and tetragonal $BiVO_4$ with scheelite structure and their photocatalytic properties. Chemistry of Materials 2001; 13(12): 4624–4628.
27. Li Y, Dong S, Wang Y, *et al.* Reduced graphene oxide on a dumbbell-shaped $BiVO_4$ photocatalyst for an augmented natural sunlight photocatalytic activity. Journal of Molecular Catalysis A Chemical 2014; 387: 138–146.
28. Peng F, Ni Y, Zhou Q, *et al.* Construction of ZnO nanosheet arrays within $BiVO_4$ particles on a conduc-

tive magnetically driven cilia film with enhanced visible photocatalytic activity. Journal of Alloys and Compounds 2017; 690: 953–960.
29. Yu C, Dong S, Feng J, *et al.* Controlled synthesis of uniform $BiVO_4$ microcolumns and advanced visible-light-driven photocatalytic activity for the degradation of metronidazole-contained wastewater. Environmental Science and Pollution Research International 2014; 21(4): 2837–2845.
30. Geng Y, Zhang P, Li N, *et al.* Synthesis of Co doped $BiVO_4$ with enhanced visible-light photocatalytic activities. Journal of Alloys and Compounds 2015; 651: 744–748.
31. Li J, Guo Z, Liu H, *et al.* Two-step hydrothermal process for synthesis of F-doped $BiVO_4$ spheres with enhanced photocatalytic activity. Journal of Alloys and Compounds 2013; 581: 40–45.
32. He Z, Shi Y, Chao G, *et al.* $BiOCl/BiVO_4$ p–n heterojunction with enhanced photocatalytic activity under visible-light irradiation. Journal of Physical Chemistry C, 2014, 118(1): 389–398.
33. Li R, Han H, Zhang F, *et al.* Highly efficient photocatalysts constructed by rational assembly of dual-cocatalysts separately on different facets of $BiVO_4$. Energy & Environmental Science, 2014, 7(4): 1369.
34. Song L, Pang Y, Zheng Y, *et al.* Design, preparation and enhanced photocatalytic activity of porous $BiOCl/BiVO_4$ microspheres via a coprecipitation-hydrothermal method. Journal of Alloys and Compounds 2017; 710: 375–382.
35. Zhou L, Wang W, Liu S, *et al.* A sonochemical route to visible-light-driven high-activity $BiVO_4$ photocatalyst. Journal of Molecular Catalysis A: Chemical 2006; 252(1-2): 120–124.
36. Jun YW, Choi JS, Cheon J. Shape control of semiconductor and metal oxide nanocrystals through nonhydrolytic colloidal routes. Angewandte Chemie (International ed. in English) 2006; 45(21): 3414–3439.
37. Yu J, Kudo A. Effects of structural variation on the photocatalytic performance of hydrothermally synthesized $BiVO_4$. Advanced Functional Materials 2006; 16(16): 2163–2169.
38. Yu J, Kudo A. Hydrothermal synthesis and photocatalytic property of 2-dimensional bismuth molybdate nanoplates. Chemistry Letters 2005; 34(11): 1528–1529.
39. Liu J, Wang H, Wang S, *et al.* Hydrothermal preparation of $BiVO_4$ powders. Materials Science and Engineering: B 2003; 104(1-2): 36–39.
40. Li Z, Chen D, Jiao X. Monoclinic structured $BiVO_4$ nanosheets: Hydrothermal preparation, formation mechanism, and coloristic and photocatalytic properties. The Journal of Physical Chemistry. B 2006; 110(6): 2668–73.
41. Dong S, Yu C, Li Y, *et al.* Controlled synthesis of T-shaped $BiVO_4$ and enhanced visible light responsive photocatalytic activity. Journal of Solid State Chemistry 2014; 211(5): 176–183.
42. Wetchakun N, Chaiwichain S, Inceesungvorn B, *et al.* $BiVO_4/CeO_2$ nanocomposites with high visible-light-induced photocatalytic activity. ACS Applied Materials & Interfaces 2012; 4(7): 3718–3723.
43. Guo Y, Xia Y, Ma F, *et al.* Additive-free controllable fabrication of bismuth vanadates and their photocatalytic activity toward dye degradation. Applied Surface Science 2010; 256(7): 2215–2222.
44. Zhang A, Zhang J, Cui N, *et al.* Effects of pH on hydrothermal synthesis and characterization of visible-light-driven $BiVO_4$ photocatalyst. Molecular Catalysis 2009; 304(1): 28–32.
45. Xu X, Zou Q, Yuan Y, *et al.* Preparation of $BiVO_4$-graphene nanocomposites and their photocatalytic activity. Journal of Nanomaterials 2014; 2014: 1–6.